Probing the Organization of Photosystem II in Photosynthetic Membranes by Atomic Force Microscopy †

ARTICLE *in* BIOCHEMISTRY · FEBRUARY 2008

Impact Factor: 3.02 · DOI: 10.1021/bi7017877 · Source: PubMed

Probing the Organization of Photosystem II in Photosynthetic Membranes by Atomic Force Microscopy†

Helmut Kirchhoff,*,‡ Steven Lenhert,§ Claudia Büchel,|| Lifeng Chi,⊥ and Jon Nield▽

Institut für Botanik, Schlossgarten 3, D-48149 Münster, Germany, Institut für NanoTechnologie, Forschungszentrum Karlsruhe GmbH, P.O. Box 3640, D-76021 Karlsruhe, Germany, Institute of Molecular Biosciences, University of Frankfurt, Siesmayerstrasse 70, D-60323 Frankfurt, Germany, Physikalisches Institut, Wilhelm-Klemm-Strasse 10, D-48149 Münster, Germany, and Division of Molecular Biosciences, Wolfson Laboratories, Imperial College London, South Kensington, London SW7 2AZ, United Kingdom

Received August 31, 2007; Revised Manuscript Received October 26, 2007

ABSTRACT: Efficient photosynthetic energy transduction and its regulation depend on a precise supramolecular arrangement of the plant photosystem II (PSII) complex in grana membranes of chloroplasts. The topography of isolated photosystem II supercomplexes and the supramolecular organization of this complex in grana membrane preparations are visualized by high-resolution atomic force microscopy (AFM) in air in tapping mode with an active feedback control to minimize tip−sample interactions. Systematic comparison between topographic characteristics of the protrusions in atomic force microscopic images and well-established high-resolution and freeze-fracture electron microscopic data shows that the photosystem II organization can be properly imaged by AFM in air. Taking the protruding water-splitting apparatus as a topographic marker for PSII, its distribution and orientation in isolated grana membrane were analyzed. For the latter a new mathematical procedure was established, which revealed a preference for a parallel alignment of PSII that resembles the organization in highly ordered semicrystalline arrays. Furthermore, by analyzing the height of grana membrane stacks, we conclude that lumenal protrusions of adjacent photosystem II complexes in opposing membranes are displaced relative to each other. The functional consequences for lateral migration processes are discussed.

One of the most complex structured biomembranes in nature is the thylakoid membrane system present within chloroplasts of higher plants. Part of this membrane system forms strictly stacked grana membranes interconnected by unstacked stroma lamellae. For recent models see refs *1* and *2*. The resulting subcompartmentation in stacked and unstacked regions has been shown to be the basis for a pronounced lateral segregation of the photosynthetic protein supercomplexes which are embedded in the thylakoid membrane (*3*). The main population of photosystem (PS)[1] II and its light-harvesting complex (LHC) II antenna system is concentrated in the grana thylakoids, whereas PSI with its concomitant LHCI and the ATPase cannot enter the stacked regions, most probably due to protrusions on their stromal side, and are found in the unstacked stroma lamellae. The localization of the cytochrome (cyt) b_6f complex has not yet been clarified. It is assumed that this complex is evenly distributed throughout the thylakoid membranes (*3*). Intensive research over the past few decades has led to detailed knowledge of the molecular architecture of the individual photosynthetic protein complexes (*4*). A deeper understanding of the functionality of these complexes on the molecular level is now possible by combining the structural information with the huge amount of biophysical (e.g., spectroscopic) data. In particular there is considerable progress on the structure−function relationship for PSII (*5*), PSI (*6*), and LHCII (*7*, *8*). The molecular architecture of photosynthetic protein complexes reveals a pronounced structural complexity; i.e., the PSII complex in grana thylakoids forms a dimeric supercomplex with at least two strongly bound LHCII trimers (*9*, *10*). Each PSII monomer in this supercomplex contains more than 20 subunits and binds more than 100 cofactors.

It is expected that the precise arrangement of many protein complexes (supramolecular level) in grana membranes determines the light-harvesting function of PSII and its regulation and lateral diffusion processes. From functional and structural studies there is evidence that PSII, cyt b_6f complexes, and LHCII are not randomly organized in grana thylakoids but could form structured arrangements (*11*−*13*), indicating the operation of ordering forces in grana thyla-

† H.K. is supported by the Deutsche Forschungsgemeinschaft (Grants KI818/2-1, KI818/2-2, KI818/3-1, and KI818/4-1). C.B. gratefully acknowledges an EU grant (Intro 2, MRTN-CT-2003-505069). J.N. currently holds a Royal Society University Research Fellowship.

* To whom correspondence should be addressed. Phone: +49 251 832482. Fax: +49 251 8323823. E-mail: kirchhh@uni-muenster.de.

‡ Institut für Botanik.

§ Forschungszentrum Karlsruhe GmbH.

|| University of Frankfurt.

⊥ Physikalisches Institut.

▽ Imperial College London.

[1] Abbreviations: AFM, atomic force microscopy; BBYs, isolated grana thylakoids; chl, chlorophyll; cyt, cytochrome; EDTA, ethylenediaminetetraacetate; EM, electron microscopy; HEPES, *N*-2-hydroxyethylpiperizine-*N*′-2-ethanesulfonic acid; NNDF, next neighbor distribution function; NNADF, next neighbor angle distribution function; LHC, light-harvesting complex; PS, photosystem; TRIS, tris(hydroxymethyl)aminomethane.

10.1021/bi7017877 CCC: $40.75
Published on Web 12/08/2007

koids. In addition, at least under certain conditions, PSII complexes can further organize into highly ordered 2D crystals (*9*). These observations allude to a certain flexibility in the supramolecular protein arrangement, which in turn could modulate photosynthetic function. This would open up the possibility for a regulative adjustment of the photosynthetic machinery, i.e., upon environmental changes by changing the protein organization in the membrane (*14*). At this point we can only speculate about the functional significance of supramolecular protein ordering. It is likely that the light-harvesting efficiency of photosystem II or diffusion of plastoquinone, phosphorylated LHCII, or photodamaged PSII is affected by the precise protein arrangement. To examine the significance of the protein organization in grana thylakoids, ultrastructural methods are required to visualize the arrangement of protein complexes.

So far, the macromolecular protein arrangement in photosynthetic membranes has been examined mainly by electron microscopic techniques, using either freeze-fracture techniques on native membranes (*15*) or negatively stained samples obtained by mild detergent treatment of thylakoids (*16*). Besides the huge number of important findings made by electron microscopy, there are several drawbacks associated with these techniques. Using freeze-fracturing, only metal replicas are examined, and for negative staining the samples have to be fixed and become dehydrated since they are analyzed under high vacuum (*17*). Thus, there is a risk of plastic deformation of the protein complexes. An alternative to study the ultrastructure of biomembranes with molecular resolution is atomic force microscopy (AFM), which was established in the 1980s (*18*). In extension to electron microscopic techniques the height of samples can be precisely measured with AFM. In the past two decades this technique has become a key tool in the life sciences (*19*). Some advantages are a high signal-to-noise ratio, a fast sample preparation, and the possibility of imaging the probe in air or aqueous solutions under physiological conditions. The technique was improved for studying soft biomolecules by the introduction of the dynamic tapping mode and a so-called "Q-control" (*20*). The Q-control is an active feedback circuit which reduces the forces between the AFM tip and the sample and therefore minimizes the deformation induced by the AFM tip. Direct comparisons between images of DNA−protein complexes using the same tip taken with and without Q-control reveal that soft molecules imaged without Q-control appear lower and wider than expected, while images taken using Q-control show features closer to known dimensions (*21*). Recently high-resolution AFM was applied on chemically fixed thylakoids (*22*) and on the photosynthetic membranes of purple bacteria (*23*, *24*). For a recent review see ref *25*. In the first study the protein organization of PSI and the ATPase was analyzed in stroma lamellae, grana margins, and end membranes with intact thylakoid membranes after immunolabeling. Furthermore, low-resolution AFM images of isolated grana thylakoids were also recently published (*26*, *27*) in which the degree of stacking and the mean height of grana membranes were measured. In this work we study the molecular organization of PSII complexes within the stacked regions of unfixed grana membranes in air by AFM with a lateral resolution of about 4 nm. The protrusion of the water-splitting apparatus of PSII was used as a topographical feature to identify the position and orientation of individual PSII complexes in AFM micrographs. Furthermore, the spacing of stacked grana membranes was analyzed.

MATERIALS AND METHODS

Preparation of Isolated Grana Membranes. Thylakoids were isolated from 6 week old spinach plants (*Spinacea oleracea* var. *polka*) grown hydroponically. The plants were grown at 13−17 °C with a photoperiod of 10 h and about 300 μmol of quanta m^{-2} s^{-1}. Isolated grana thylakoids (BBYs) were prepared according to ref *28* with modifications described in ref *13*. The chlorophyll *a*/*b* ratio of the preparation determined according to ref *29* was 2.2 ± 0.1, which is typical for grana core membranes (*30*). The activity of the preparation measured as light-saturated oxygen evolution in the presence of the PSII acceptor 1,4 dimethylbenzoquinone (1.5 mmol L^{-1}) was 306 μmol O_2 (mg of chlorophyll)$^{-1}$ h^{-1}.

PSII Supercomplex and LHCII Trimer Preparation. Supercomplexes of PSII from market spinach were separated on sucrose gradients after solubilization of thylakoids with 20 mM β-dodecyl maltoside according to ref *31*. Chlorophyll was determined as described above, yielding a chl *a*/*b* ratio of 3.1. Trimeric LHCII was isolated from spinach as described in ref *32*. The chlorophyll *a*/*b* ratio of 1.41 as well as the maxima in the absorption spectrum at 435, 473, 652, and 675 nm and the emission maximum in 77 K fluorescence spectra at 680 nm with a small satellite at 740 nm are indicative of the purity of the preparation.

Spectroscopy. The contents of cytochrome *f*, b_6 and b_{559} were determined from chemical difference absorption spectra measured between 520 and 580 nm with a Hitachi U3010 spectrometer (bandpath 1 nm, scan speed 120 nm min^{-1}, average of 10 scans) as described previously (*33*). BBY membranes were incubated in 10 mM KCl, 50 μM EDTA, 330 mM sorbitol, 20 mM HEPES (pH 7.6, KOH), and 0.03% β-dodecyl maltoside. Starting from completely oxidized cytochromes (in the presence of 1 mM ferricyanide), the redox potential was stepwise decreased by the addition of 5 mM sodium ascorbate and a few grains of sodium dithionite. The resulting difference spectra (sodium ascorbate minus ferricyanide and sodium dithionite minus sodium ascorbate) were fitted with reference spectra as described in ref *33*, which gave the maximal absorption changes of the cytochromes. From these values the concentrations of the cytochromes were calculated and correlated with the chlorophyll concentration. For cyt b_{559} a recently determined extinction coefficient of 25.1 mM^{-1} cm^{-1} at 560 nm (*34*) was used.

The content of P700 was deduced from light pulse induced absorption spectra at 810 nm minus 860 nm as recently described (*35*). BBY membranes were incubated in 5 mM $MgCl_2$, 30 mM KCl, 50 mM citrate (pH 4.8, KOH), 0.2% β-dodecyl maltoside, 100 μM methylviologen, and 10 mM sodium ascorbate. The maximal absorption changes induced by a 200 ms saturating light pulse (about 6000 μmol of quanta m^{-2} s^{-1}) was determined to calculate the total P700 content (*35*).

Scanning Force Microscopy. Samples were prepared by placing a 50 μL drop of stacked grana membranes on a freshly cleaved mica surface (~7 × 7 mm) for 2 min prior

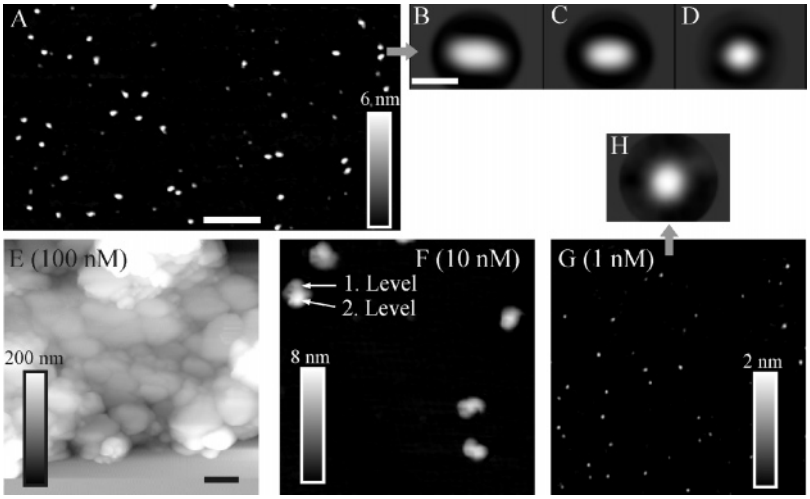

FIGURE 1: AFM micrographs and their analysis of LHCII−PSII supercomplexes and trimeric LHCII. (A) Isolated PSII supercomplexes. (E−G) isolated LHCII trimers. The numbers in parentheses give the chlorophyll concentrations. (B−D) Single-particle analysis of PSII supercomplexes. A total of 501 particles were analyzed. (H) Single-particle analysis of LHCII trimers (123 particles). Lateral dimensions deduced for the particles are summarized in Table 1. For further details, see the text. Scale bars: (A, E) 200 nm, (B) 20 nm. Scale bar in (E) also for (F) and (G).

to rinsing 10 times (100 μL/rinse) with Millipore water (resistivity 18.2 MΩ cm) to remove the buffer. The bulk water was then quickly removed from the mica surface by a nitrogen stream, and then the sample was left under the nitrogen stream for 2 min. AFM was carried out in tapping mode in air (Digital Instruments, Dimension 3000, Santa Barbara, CA) equipped with an external Q-control module (Nanoanalytics). Silicon cantilevers were used (Nanosensors) with resonant frequencies of 250−350 kHz, nominal spring constants of ∼42 N/m, and tip radii of <10 nm. The Q-control was tuned to the maximum Q-factor that allowed stable imaging to minimize the force induced on the samples by the tip.

Single-Particle Image Analysis. AFM images had an inherent resolution of 3.9 nm, and 4-fold oversampling was found to be necessary for successful image conversion. Datasets thus had a sampling frequency of 4.875 Å per pixel and were composed of protein complexes floated out into 2D image boxes of either 40 × 40 or 52 × 52 pixels (PSII) or 64 × 64 pixels (LHCII). Dataset compilation was by automatic selection routines in "boxer", a module of the EMAN software package (v1.7; *36*), followed by interactive removal of clearly false coordinate identification, i.e., empty images. All subsequent image processing was performed using the Imagic-5 environment (Image Science GmbH, Berlin). Four datasets corresponding to isolated PSII particles, TRIS-treated PSII particles, and grana membranes were subjected to reference-free alignment, followed by multivariate statistical analyses, to give initial 2D class averages that were then iteratively refined to obtain the final averages, subpopulations, and statistics (*17*, *37*).

RESULTS

For the visualization of the photosystem II arrangement in grana thylakoids by AFM, the AFM tip must have access to the surface of a grana disk. Samples which fulfilled this precondition were isolated grana thylakoid membranes prepared according to the BBY protocol (*28*). Also advantageous for the AFM technique was to ensure that the BBY method produced flat, paired membrane stacks, similar to the situation in the native membrane (*38*), which originate from the core region of grana thylakoids. Furthermore, BBY membranes must be made to orient inside out, implying that the protrusions of the water-splitting apparatus of PSII point toward the AFM tip and can therefore be used as a topographic feature to identify PSII complexes contained within the lipid bilayer. Last, evidence was found from previous freeze-fracture electron microscopy that the arrangement of PSII in BBYs is virtually indistinguishable from that of intact thylakoids (*13*). It was therefore concluded that BBYs are suitable for the visualization of the PSII organization by AFM. In principle, the cytochrome *f* subunit of the cyt b_6f complex and the extrinsic parts of PSI protrude several nanometers out of the membrane surface (*4*). However, from chemical difference absorption spectra it was deduced here that there was a chlorophyll to cyt b_{559} ratio of 219 ± 8 and a ratio of 3421 ± 571 for cyt *f* (three independent determinations). No cytochrome b_6 signal was detected. Assuming that each PSII monomer binds one cyt b_{559} (*34*), a ratio of more than 16 PSII monomers to 1 *cyt* b_6f complex is concluded. In addition, from light pulse induced difference absorption spectroscopy of P700, we deduced a chlorophyll to PSI stoichiometry of 6560 ± 1080 (three determinations), giving a PSII/PSI ratio of about 30. This indicates that the grana preparation reported here is highly depleted in both cyt *bf* complexes and PSI, typical for BBY membranes (*38*).

AFM of Isolated PSII Supercomplexes and LHCII Trimers. To test the applicability of the AFM technique to visualize photosynthetic protein complexes in air, the structurally well-defined LHCII−PSII supercomplex (*9*, *10*) and the trimeric LHCII complex (*7*, *8*), both purified from spinach, were chosen as model systems (Figure 1). Single-particle analysis of isolated PSII supercomplexes (Figure 1A) reveals three particle classes (Figure 1B−D). Their lateral dimensions are summarized in Table 1. The information about the height was perturbed during this analysis and prevented direct correlation between the lateral dimensions and height. Therefore, the height of the particles was measured separately. A height histogram (not shown) reveals two types of

Table 1: Dimensions of Isolated PSII Supercomplexes and LHCII Trimers

Figure	lateral dimension (nm)	height (nm)	lit. height (nm)	height ratio, AFM/lit. (%)
1B	32.3 × 18.9; 35% (n = 173)	6.5 ± 0.6 (72%)[a]	9.5[b] (PDB file 1S5L)	68
1C	26.4 × 18.2; 42% (n = 208)	6.5 ± 0.6 (72%)[a]	9.5[b] (PDB file 1S5L)	68
1D	19.1 × 17.4; 24% (n = 120)	2.8 ± 0.6 (29%)[a]		
1G	19.5 × 20.9 (n = 123)	2.9 ± 0.4 (n = 82)	4.8 (*55*)	60
1F, 1.Level		3.2 ± 0.6 (n = 28)	4.8 (*55*)	67
1F, 2.Level		6.3 ± 0.8 (n = 28)		

[a] A total of 795 particles were analyzed. [b] The height is estimated from the cyanobacterial PSII complex with extrinsic subunits of the water-splitting apparatus removed.

particles of about 2.8 and 6.5 nm height. Comparing the abundance of lateral dimensions and height, it was concluded that the particles in Figure 1B,C are 6.5 nm high and the particle in Figure 1D is 2.8 nm high (Table 1). This assignment was confirmed by measuring the lateral dimension and height of randomly selected individual particles in the AFM images (not shown). It is likely that the particle shown in Figure 1B represents the dimeric LHCII−PSII supercomplex because the lateral dimensions are in good agreement with a higher plant supercomplex of 33.0 × 16.5 nm (*39*). Single-particle and height analysis of 453 objects from TRIS-treated supercomplexes (not shown) reveals that 24% of the particles have dimensions of 30.9 × 21.1 × 7.1 ± 0.5 nm (length × width × height) and 73% dimensions of 21.5 × 18.5 × 3.1 ± 0.7 nm. TRIS treatment removes extrinsic subunits (PsbO, PsbP, and PsbQ) of the water-splitting apparatus (*40*, *41*). The increased abundance of smaller particles and the decrease in larger particles (compare with Table 1) indicate a disintegration of PSII supercomplexes into smaller subparticles by the TRIS treatment, which was already reported (*42*). The observation that TRIS treatment did not reduce the height of the supercomplex gives strong evidence that in untreated samples extrinsic water-splitting subunits were already absent. The lateral dimension of particle C is significantly smaller, indicating that a fraction of the supercomplexes have lost subunits. This had previously been observed in electron microscopic studies of isolated supercomplexes (*39*).

Due to the fact that the height of the object in Figure 1D is significantly lower than that of the objects in Figure 1B,C (Table 1), this particle most likely represents free LHCII complexes (*7*, *10*). A deeper analysis of isolated LHCII trimers is presented in Figure 1. Interestingly, at high protein concentrations (Figure 1E), extended stacks of flat patches were formed which can be higher than 200 nm. This 2D and 3D self-aggregation of trimeric LHCII complexes induced by high protein concentrations is well established in the literature (see, e.g., ref *32*). Smaller protein patches were produced simply by dilution. At 10 nM chlorophyll (Figure 1F) separated patches of 100−200 nm diameter occurred with two discrete height levels (indicated by arrows in Figure 1F) of 3.2 and 6.3 nm (Table 1). Further dilution leads to formation of one type of (small) particle (Figure 1G,H) with dimensions of about 19.5 × 20.9 × 3 nm (Table 1). The size of this object is in good accordance with the sizes of particle 1D, supporting the interpretation that in AFM micrographs of the PSII supercomplex free LHCII complexes were present.

To summarize, in AFM micrographs of dried samples, the lateral dimensions of intact isolated LHCII−PSII supercomplexes (Figure 1B) are not significantly altered. Unlike that of the PSII complex, the lateral size of isolated trimeric LHCII is significantly larger than expected from high-resolution data (*7*), as assuming that the complex is surrounded by a detergent shell the diameter should be 11−12 nm (8 nm + 2 × 1.7 nm). Most likely this enlargement is caused by a tip−sample convolution effect (see, e.g., ref *43*). It is noteworthy that the convolution effect is much more pronounced for smaller objects (i.e., LHCII) than for larger ones (i.e., PSII supercomplexes) (*43*). The comparison of the height deduced by AFM in air with literature data (summarized in Table 1) reveals 30−40% shrinkage of the protein complexes. However, the height of a stack of two LHCII layers is almost the double of one LHCII layer (Figure 1F, Table 1), indicating that taking the height from AFM as an intrinsic measurement allows for relative comparisons of height values. This will be relevant for the organization of grana stacks presented below.

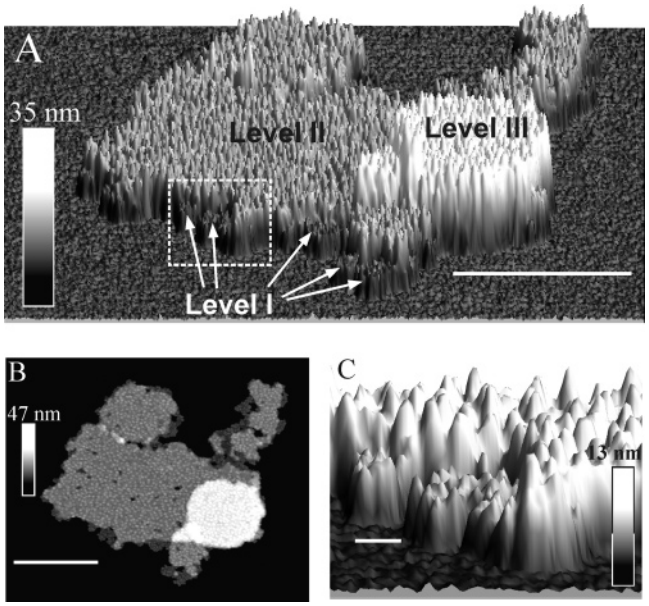

FIGURE 2: (A) 3D representation of an AFM image in air from stacked grana membranes isolated from spinach thylakoids. I, II, and III indicate discrete height levels. The white box indicates the region shown enlarged in (C). (B) 2D representation of the same AFM image. Scale bars: (A, B) 500 nm, (C) 50 nm.

Scanning Force Microscopy of Isolated Grana Thylakoids. Figure 2 shows an example of an AFM micrograph from isolated grana membranes. The 3D representation (Figure 2A) reveals steep increases in height to three different plateaus (levels I−III). Each plateau is crowded with protruding structures. From a statistical analysis it was found that 9% of the membranes have a mean height of 6.4 nm

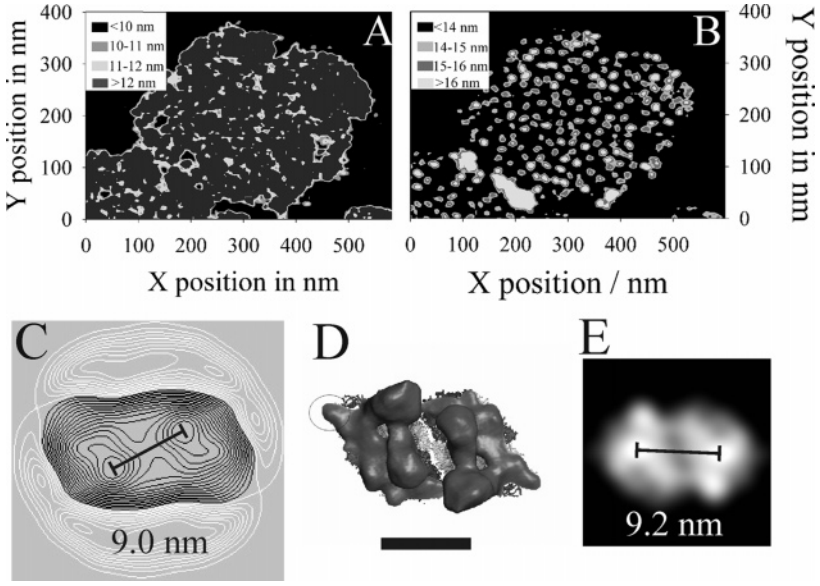

FIGURE 3: Topographical images of a grana area (area in the upper part of Figure 2B). (A) Bilayer level (see the text for the definition). (B) Protrusion level, which is about 2 nm higher than the bilayer level. Clearly separated protrusions with a height of 4−6 nm are visible. (C) Result of a single-particle analysis (566 particles) of the objects in the protrusion level (for example, see Figure 3B). (D) High-resolution structure of the lumenal part of the PSII dimer (PDB file 1S5L). Only the part which protrudes ~4 nm from the bilayer level is shown, together with an overlay of the similar density resolved at 1.7 nm resolution from cryo-EM-derived data (*45*). (E) Low-resolution 2D projection deduced by mathematical filtering from the cyanobacterial PSII underlying coordinates of (D). The resolution of ~4 nm produced by the filtering was chosen as similar to the resolution of our AFM images. For further details, see the text. The scale bar in (D) is 10 nm.

(level I), 73% a mean height of 11.9 nm (level II), and 18% a mean height of 23.2 nm (level III), which is in agreement with our previous data (*26*). The maximal height values for each level are 8.6 ± 0.4 nm (level I), 14.8 ± 0.8 nm (level II), and 26.7 ± 0.7 nm (level III). It is reasonable to assume that the three levels represent one single grana membrane, a stack of two membranes, and a stack of four membranes, respectively. It follows that most BBY membranes consist of a stack of two grana disks, which was also deduced from electron microscopic studies (*38*). The diameter of a grana disk has been observed to be 350−600 nm (*15*). The patches shown in the upper part and level III in the 2D representation (Figure 2B) are in accordance with these dimensions. However, the remaining membrane is significantly larger. This enlargement might be explained by the lateral fusion of several grana membranes by dilution of BBYs in detergent-free buffers either in solution or at the mica surface. Recently we directly observed the lateral fusion of BBYs on glass by confocal laser scanning microscopy (unpublished results), supporting the second alternative. Clearly BBYs have a high tendency to fuse together.

All AFM micrographs from grana thylakoids revealed a characteristic dense packing of protruding particles (e.g., see Figure 2). For a deeper analysis, these protrusions were visualized by the following procedure. First, the lowest height level of a grana patch was determined (light gray colors in Figure 3A). This level should represent the level of the lipid bilayer and/or the level of LHCII complexes ("bilayer level"). In stacked control membranes the height of this level was between 9.5 and 11.5 nm. In the next step the topography of the AFM image higher than 2 nm relative to the bilayer level was visualized (gray colors in Figure 3B) ("protrusion level"). We chose a value of 2 nm given that the lumenal protrusions of LHCII are not higher than 1 nm (*7*). Structures higher than 2 nm relative to the bilayer level should therefore represent exclusively PSII due to the fact that the BBY preparation contains mostly only PSII and LHCII (see above). Clearly separated particles with a roughly elliptical shape were recognized in the protrusion level (Figure 3B). The single-particle analysis of these objects resulted in one particle average type shown in Figure 3C. The lateral dimensions of this structure are about 22 nm × 13 nm and are characterized by two peaks separated by about 9 nm. To verify that this particle represents the lumenal part of photosystem II, it was compared with a high-resolution structure of the dimeric complex from cyanobacteria (*44*; PDB data file 1S5L). In this way, the lumenal density that protrudes out by 2 nm from the bilayer level was extracted from the published structure (the underlying PDB coordinates in Figure 3D) and filtered down to a resolution of 4 nm (Figure 3E), which corresponds to the resolution of our AFM micrographs. The resulting particle has a size of about 20 nm × 14 nm, whereas two density peaks (corresponding mainly to the extrinsic loops of CP47 and CP43 and the PsbO, PsbV, and PsbU gene products engaging the water-splitting apparatus) are separated by 9.2 nm. It is noteworthy that at this resolution the structure of the lumenal protrusions of the cyanobacterial PSII is very similar to that of higher plants. The correlation between the dimensions of the objects in Figure 3C,E gives strong evidence that the particles in the protrusion level (Figure 3B) represent the lumenal part of dimeric photosystem II complexes. Further evidence for this interpretation comes from the height of these protrusions relative to the bilayer level for levels II and III (see Figure 2A for the definition of the levels), which is 4.8 ± 0.8 and 4.7 ± 0.7 nm. These values are slightly lower than the expected 5.2 nm deduced from electron microscopic studies on higher plant supercomplexes (*45*). In contrast, the height for level I is significantly lower (2.6 ± 0.5 nm), which is visualized in the enlarged 3D representation in Figure 2C.

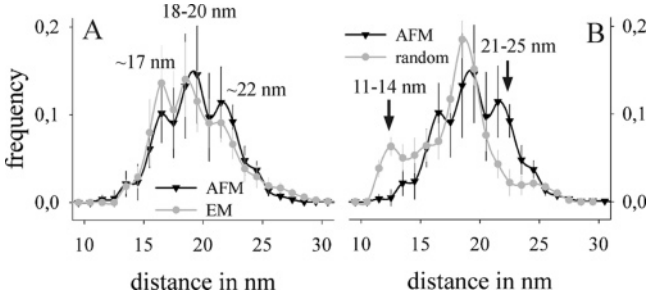

FIGURE 4: (A) Comparison of next neighbor distribution analysis of the particles in the protrusion level of grana membranes (AFM) with electron microscopic data. The data represent the mean of eight different grana patches with their standard error of the mean. Gray circles: NNDF data deduced from an electron microscopic analysis taken from spinach grana thylakoids grown under the same conditions (*13*). Note the similar pattern indicating a close correlation in arrangement of PSII complexes. (B) Comparison of AFM data with a pure random PSII distribution taken from ref *13*. For further details, see the text.

This protrusion may represent the stromal side of photosystem II. The density of the protruding structures in levels II and III is $1731 \pm 55\ \mu m^{-2}$, which is in good agreement with the PSII density of $1701 \pm 49\ \mu m^{-2}$ deduced from electron microscopic images of freeze-fractured thylakoid membranes (so-called EF particles) prepared from spinach plants grown under the same conditions (*13*).

Height analysis of TRIS-treated grana membranes and the comparison with control membranes (not shown) reveal a lower abundance of height values around 13.4 nm (level II) and 25.1 nm (level III) and a higher abundance of values around 9.8 and 21.6 nm in TRIS-treated samples. In contrast to the missing effect of TRIS treatment in isolated LHCII−PSII supercomplexes (see above), this height reduction of about 3.5 nm indicates the presence of the extrinsic subunits of the water-splitting apparatus in isolated grana membranes. The value of 3.5 nm is slightly lower than expected for the height of extrinsic lumenal subunits of PSII (3.8 nm, *45*).

In summary, the topographic characteristics of the protruding structures in levels II and III and their density as well as the height reduction after TRIS treatment gave strong evidence that these objects represent the lumenal protrusion of PSII. Most likely level I corresponds to one grana membrane with the stromal side facing toward the AFM tip, whereas levels II and III correspond to a stack of two and four membranes in which the lumenal side is facing the tip, respectively (see also Figure 7).

PSII Arrangement in Grana Thylakoids. The above results indicate that the particles in the protrusion level in grana thylakoids represent the lumenal part of dimeric PSII complexes. This opens the possibility to use this topographic feature to analyze the supramolecular organization of this complex in grana membranes. To test whether the lateral membrane organization is affected by using dried samples or by the AFM technique, a next neighbor distribution analysis was used to compare the PSII distribution deduced from AFM images with a distribution derived from well-established electron microscopic images of freeze-fractured thylakoid membranes. The next neighbor distribution function (NNDF) expresses the probability of finding an adjacent particle at a given distance and enables the objective comparison of two distributions (*46*). For the PSII distribution from cryo-EM micrographs (Figure 4A) recently published data using the same plant material grown under identical conditions were used (*13*). Comparing the next neighbor distribution between cryo-EM and AFM (Figure 4A) reveals no significant differences. In particular characteristic peaks in the distributions (indicated in Figure 4A) occurred at almost the same positions. These peaks are fingerprints of a given PSII distribution in the membrane. Noteworthy significant differences are apparent when AFM (or EM) data are compared with a purely random PSII distribution (Figure 4B) generated by computer simulations (data from ref *13*). A clear shift from shorter distances (11−14 nm) to longer distances was apparent in the AFM distribution. This shift of about 10 nm could represent an organization in which adjacent PSII complexes are spaced by trimeric LHCII complexes. The results suggest that imaging grana membranes by AFM in air does not significantly alter the spacing and lateral organization of PSII.

An advantage of the AFM technique is its high signal-to-noise ratio. In addition to determining the position and size of PSII particles, it was possible to deduce their orientation in grana membranes due to their elliptical shape. This is illustrated in Figure 5. Figure 5A shows the height profile of the protrusion level of the grana patch in Figure 2 (level II). The position and orientation of individual elliptical particles of the protrusion level were fitted with the PSII contour extracted from the single-particle analysis (Figure 3C). This leads to Figure 5B. To analyze the orientation of the PSII complexes in Figure 5B, we developed a new mathematical procedure which measured the angle of a given particle relative to its nearest neighbor. We have called this the *next neighbor angle distribution function* (NNADF) in analogy to NNDF. Figure 6 (hatched histogram) shows the NNADF for the distribution shown in Figure 5B. Note that the AFM tip geometry or scanning process itself may produce an artificial angle distribution. We analyzed this by calculating the NNADF of the isolated PSII supercomplexes which were imaged with the same tip and settings and under the same conditions as the grana thylakoids. It can be assumed that this represents a pure random distribution. Therefore, the NNADF of isolated PSII (Figure 6, gray histogram) can be used to analyze the scan-angle dependency of the AFM apparatus. The dashed line indicates the expected frequency for an equal distribution, i.e., a pure random orientation. For isolated PSII the angle distribution is almost random except for a slightly increased population of angles between 0° and 10° and depopulation of angles between 50° and 75°. These deviations from an equal distribution should represent the angle dependency of the AFM setup. However, compared to this distribution, significant deviation is apparent in the PSII orientation in BBY membranes. In particular, it appears obvious that in grana thylakoids the PSII complexes are arranged more parallel (an increase in angles between 0° and 25°) than perpendicular (a decrease in angles between 70° and 90°) to each other.

DISCUSSION

Applicability of AFM in Air To Visualize PSII Complexes. In this study dried samples were used to analyze the PSII organization in grana thylakoids. An advantage of measuring with dried samples is that the mobility of membrane proteins should be significantly reduced. AFM images taken from dried samples are a kind of frozen snapshot of the protein

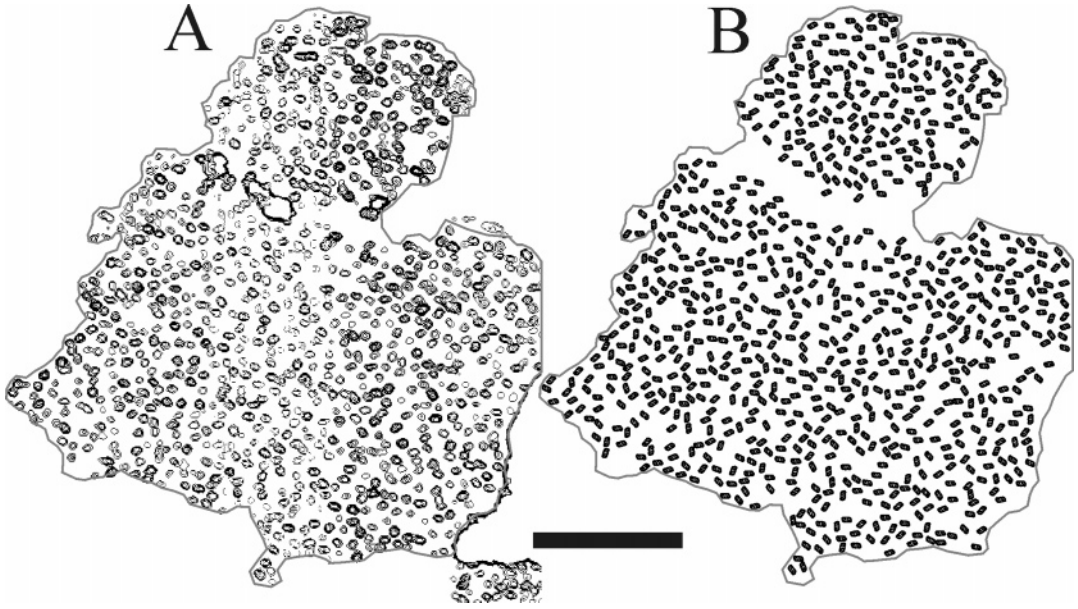

FIGURE 5: Fitting the PSII structure deduced from single-particle analysis (Figure 3C) to the protrusions of a grana membrane. (A) Protrusions (2 nm above the bilayer level) of the grana patch shown in Figure 2 (level II). For each protrusion the position and the orientation of the PSII structure deduced from a single-particle analysis of the same membrane patch (Figure 3C) were fitted by hand given (B). Scale bar 250 nm.

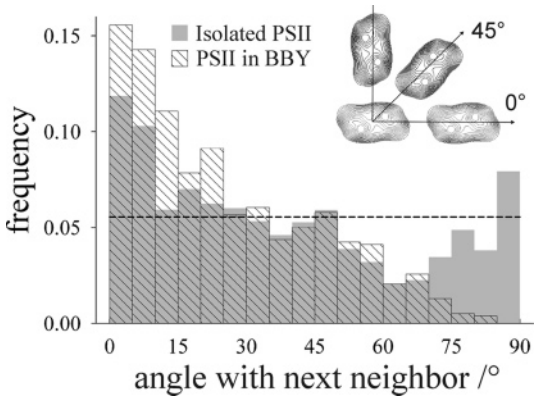

FIGURE 6: Next neighbor angle distribution analysis. From a given particle the NNADF measures the angle with its next neighbor, taking the long axis as 0°. The definition of the angles is depicted in the inset. The analysis was applied either for isolated PSII complexes (gray bars) or for the protrusions in a grana membrane (hatched bars). Note the redundancy of angles greater than 90°. For example, angles of 135°, 225°, or 315° are not distinguishable from the 45° angle. Thus, the angles higher than 90° are transformed to angles between 0° and 90°. The dashed line indicates the expected frequency for a pure random angle distribution, i.e., no preference in orientation to the next neighbor. For further details, see the text.

organization. In principle, photosynthetic protein can diffuse with a high rate. E.g., recently we found that a fraction of chlorophyll−protein complexes in BBY membranes migrate with a diffusion coefficient of about 0.5×10^{-10} cm^2 s^{-1} (unpublished results). This value translates to a mean diffusion distance of about 140 nm s^{-1}. Given that the AFM image process is slow (e.g., 2 s per X line in Figure 2), these fast-migrating protein complexes cannot be detected and would perturb the AFM imaging process. However, an important prerequisite to analyze PSII organization in grana membranes by AFM of dried samples is that these measuring conditions do not lead to artificial membrane rearrangements. Good evidence exists that the lateral PSII organization is not significantly altered in AFM micrographs: (i) The lateral dimension of the isolated complete LHCII−PSII supercomplex is in good accordance with high-resolution data. (ii) Comparison with freeze-fracture EM data reveals no lateral shrinkage (almost the same PSII density and mean separation of neighbored complexes). (iii) Next neighbor distribution analysis (Figure 4) shows a typical pattern of distinct distances as in freeze-fracture EM. Thus, we conclude that AFM of dried grana membranes is an adequate tool for analyzing the static PSII organization. However, significant deviations were observed in the height of isolated complexes and grana membranes (see below).

Vertical Organization of PSII in Stacked Grana Thylakoids. In principle, one benefit of the AFM technique is the possibility to measure the height of samples with great accuracy. However, for isolated PSII supercomplexes and trimeric LHCII the height is 30−40% lower than expected from high-resolution data (Table 1), indicating some vertical shrinkage. In grana membranes this shrinkage is less pronounced. The maximal height of one grana membrane should be determined by the height of PSII; hence, one expected a value of 10−11 nm (*45*). The height measured by AFM is about 20% lower (8.6 nm). This reduced shrinkage may be due to a higher amount of residual water in the membranes compared to isolated complexes. However, an important finding was the almost exact doubled height value for a stack of two layers of isolated trimeric LHCII compared to one layer (Table 1). Thus, the height deduced by AFM for one grana membrane can be used as an intrinsic measure for analyzing the vertical PSII organization in stacks of several grana membranes (Figure 7). Taking the maximal height of a single grana membrane, a stack of two membranes (level II in Figure 2) should be 17.2 nm, in contrast to a measured height of about 14.8 nm. This difference could be explained by a displaced arrangement of the stromal protrusions of two adjacent PSII complexes (Figure 7) which would give a maximal height of about 14.6 nm (2×8.6 nm $- 2.6$ nm), in good agreement with the measured value. A conclusion similar to that for the stromal side can be drawn

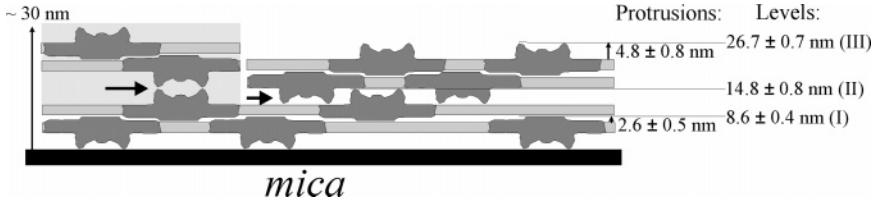

FIGURE 7: Scheme of the vertical organization of PSII−LHCII supercomplexes deduced from the AFM height measurements. Supercomplexes with reduced height because of the drying in air (see Table 1). Dark gray structures: PSII−LHCII supercomplex. Light gray bars: lipid bilayer. In stacks of two paired grana membranes, lumenal protrusions of PSII can face directly opposite each other (indicated by the arrow in the gray box in the upper left) or can be displaced relative to each other (arrow in the middle).

for a stack of two paired membranes with respect to the lumenal protrusion of PSII. From our values it is expected that a stack of two paired grana membranes (level III in Figure 2) should have a height of about 29.6 nm (2 × 14.8 nm), which is about 3 nm higher than the measured value. The simplest explanation for this reduction in height is the displacement of the water-splitting apparatus of two adjacent PSII complexes (Figure 7). For a displaced organization of the water-splitting apparatus in opposite membranes, a height value of 26.0 nm is expected (2 × 14.8 nm − 3.6 nm). Thus, the height analysis gives evidence for a dovetailed arrangement of protruding stromal and lumenal parts of PSII in neighbored grana disks. The question of whether the lumenal protrusions of opposing PSII complexes are directly facing each other or are displaced is relevant for the migration of hydrophilic lumenal proteins as well as for membrane proteins with lumenal protrusions (PSII, cyt *bf* complex). In particular, this should affect the migration of photodamaged PSII complexes to the stroma lamellae and back in the course of its repair cycle (*47*) and the diffusion of plastocyanine (*48*, *49*). It is expected that a displaced arrangement of the water-splitting apparatus as proposed from our data would hinder lumenal diffusion processes since (i) the inner width of the lumen is smaller (see Figure 7) and (ii) the number of diffusion obstacles is increased. Therefore, the removal of the water-splitting apparatus from the photodamaged PSII complex (*50*) could be important not only for the functionality of the photoinhibited complex, but also for its efficient migration to unstacked stroma lamellae in the course of the repair cycle.

Ordered PSII Organization in Grana Thylakoids. In extension to earlier results which demonstrate a nonrandom PSII positioning (*13*) and which are confirmed by the AFM data (Figure 4), the analysis in Figure 6 also reveals a tendency for an ordered parallel alignment of PSII in a seemingly randomly organized grana membrane. A parallel alignment of PSII was also observed in isolated so-called megacomplexes (dimers of LHCII−PSII supercomplexes) and in highly ordered 2D semicrystalline PSII arrays in isolated grana membranes and intact thylakoids which can be formed under certain conditions (summarized in ref *9*). Both the positional order (Figure 4) and orientational order (Figure 6) indicate that the same forces involved in 2D semicrystalline array formation are also apparent in membranes with noncrystalline organization. The results indicate that grana membranes are in a kind of "precrystalline" state in which building blocks for highly ordered crystalline organization are preformed. The factors which govern the degree of array formation are not known. Specific protein−protein interactions, i.e., between trimeric LHCII and LHCII−PSII supercomplex (*51*), or alteration in the lipid organization in the membrane bilayer is probably involved (*52*). For the latter we proposed a causal link between lateral membrane pressure, modulated by the nonbilayer HII phase of monogalactosyldiacylglycerol, and binding properties of LHCII and/or PSII which in turn trigger array formation (*52*). However, the results suggest a delicate balance of ordering and disordering forces in grana membranes which determine a flexible equilibrium in the PSII arrangement. Interestingly, evidence accumulates that 2D array formation is stress induced (*9*, *52*). Thus, supramolecular ordering seems to be correlated with an optimization of photosynthetic functions.

The functional consequences of an alignment and separation of PSII complexes are unknown. Lateral diffusion processes (proteins and or plastoquinone) or the intermolecular-dependent light-harvesting function of photosystem II could be affected. The parallel organization of PSII most likely reflects preferential interactions between LHCII at the top and bottom sides of the supercomplex, leaving the middle portion protein-free. This is important for an efficient binding and unbinding of plastoquinone/plastoquinol because the QB binding niche is localized in this region (*44*). Furthermore, efficient protein traffic is necessary for adaptation mechanisms such as state transitions (*53*) or the PSII repair cycle (*54*). Diffusion analysis gives evidence for facilitated migration of a fraction of pigment protein complexes (PSII or LHCII) in grana thylakoids, allowing for fast protein exchange between stacked and unstacked membrane regions (unpublished results). The structural basis for this fast diffusion in crowded grana membranes may be the formation of small diffusion channels which must be formed by organized protein arrangement. Parallel alignment of PSII supercomplexes could be a key factor for this kind of organization required for efficient diffusion processes in densely packed grana thylakoids. A fraction of PSII complexes in Figure 5B indeed show a chainlike arrangement.

In this study we have demonstrated visualization of the supramolecular organization of photosystem II in grana thylakoids using AFM in air. From the high accuracy with which one can map surface topography by AFM, we have concluded that the lumenal and stromal protrusions of PSII complexes in adjacent grana disks are displaced relative to each other. Furthermore, a preference for an ordered parallel arrangement of neighbored PSII complexes was detected.

REFERENCES

1. Mustárdy, L., and Garab, G. (2003) Granum revisited. A three-dimensional model—where thinks fall into place, *Trends Plant Sci. 8*, 117−122.
2. Shimoni, E., Rav-Hon, O., Ohad, I., Brumfeld, V., and Reich, Z. (2005) Three-dimensional organization of higher plant chloroplast thylakoid membranes revealed by electron tomography, *Plant Cell 17*, 2580−2586.

3. Albertsson, P. A. (2001) A quantitative model of the domain structure of the photosynthetic membrane, *Trends Plant Sci. 6*, 349−354.
4. Nelson, N., and Ben Shem, A (2004) The complex architecture of oxygenic photosynthesis, *Nat. Rev. Mol. Cell Biol. 5*, 971−982.
5. Wydrzynski, T. J., and Satoh, K. (2005) The light-driven water: plastoquinone oxidoreductase, in *Advances in photosynthesis and respiration* (Govindjee, Ed.) Vol. 22, Springer, Dordrecht, The Netherlands.
6. Melkozernov, A. N., Barber, J., and Blankenship, R. E. (2006) Light harvesting in photosystem I supercomplexes, *Biochemistry 45*, 331−345.
7. Standfuss, J., van Scheltinga, A. C. T., Lamborghini, M., and Kuehlbrandt, W. (2005) Mechanisms of photoprotection and nonphotochemical quenching in pea light-harvesting complex at 2.5 A resolution, *EMBO J. 24*, 919−928.
8. Liu, Z., Yan, H., Wang, K., Kuang, T., Zhang, J., Gui, L., An, X., and Chang, W. (2004) Crystal structure of spinach major light-harvesting complex at 2.72 A resolution, *Nature 428*, 287−292.
9. Dekker, J. P., and Boekema, E. J. (2005) Supramolecular organization of thylakoid membrane proteins in green plants, *Biochim. Biophys. Acta 1706*, 12−39.
10. Nield, J., and Barber, J. (2006) Refinement of the structural model for the photosystem II supercomplex of higher plants, *Biochim. Biophys. Acta 1757*, 353−361.
11. Lavergne, J., Bouchaud, J.-P., and Joliot, P. (1992) Plastochinone compartimentation in chloroplasts. II. Theoretical aspects, *Biochim. Biophys. Acta 1101*, 13−22.
12. Kirchhoff, H., Horstmann, S., and Weis, E. (2000) Control of the photosynthetic electron transport by PQ diffusion microdomains in thylakoids of higher plants, *Biochim. Biophys. Acta 1459*, 148−168.
13. Kirchhoff, H., Tremmel, I., Haase, W., and Kubitscheck, U. (2004) Supramolecular photosystem II organization in grana thylakoid membranes: evidence for a structured arrangement, *Biochemistry 43*, 9204−0213.
14. Nield, J., Redding, K., and Hippler, M. (2004) Remodeling of light-harvesting protein complexes in chlamydomonas in response to environmental changes, *Eukaryotic Cell 3*, 1370−1380.
15. Staehelin, L. A., and van der Staay, G. W. M. (1996) Structure, composition, functional organization and dynamic properties of thylakoid membranes, in *Oxygenic photosynthesis: The light reactions* (Ort, D. A., and Yocum, C. F., Eds.) pp 11−30, Kluwer Academic Publishers, Dordrecht, The Netherlands.
16. Boekema, E. J., van Breenen, J. F., van Roon, H., and Dekker, J. P. (2000) Arrangement of photosystem II supercomplexes in crystalline macrodomains within the thylakoid membrane of green plant chloroplasts, *J. Mol. Biol. 301*, 1123−1133.
17. Ruprecht, J., and Nield, J. (2001) Determining the structure of biological macromolecules by transmission electron microscopy, single particle analysis and 3D reconstruction, *Prog. Biophys. Mol. Biol. 75*, 121−164.
18. Binnig, G., Quate, C. F., and Gerber, C. (1986) Atomic force microscope, *Phys. Rev. Lett. 56*, 930−933.
19. Mueller, D. J., Janovjak, H., Lehto, T., Kuerschner, L., and Anderson, K. (2002) Observing structure, function and assembly of single proteins by AFM, *Prog. Biophys. Mol. Biol. 79*, 1−43.
20. Gao, S., Chi, L., Lenhert, S., Anczykowski, B., Niemeyer, C. M., Adler, M., and Fuchs, H. (2001) High-quality mapping of DNA-protein complexes by dynamic scanning force microscopy, *ChemPhysChem 6*, 384−388.
21. Pignataro, B., Chi, L. F., Gao, S., Anczykowski, B., Niemeyer, C., Adler, M., and Fuchs, H. (2002) Dynamic scanning forcemicroscopy study of self-assembled DNA-protein nanostructures, *Appl. Phys. A 74*, 447−452.
22. Kaftan, D., Brumfeld, V., Nevo, R., Scherz, A., and Reich, Z. (2002) From chloroplasts to photosystems: *in situ* scanning force microscopy on intact thylakoid membranes, *EMBO J. 21*, 6146−6153.
23. Bahatyrova, S., Frese, R. N., Siebert, C. A., Olsen, J. D., Van der Werf, K. O., Van Grondelle, R., and Niederman, R. A., Bullough, P. A., Otto, C., Hunter, C. N. (2004) The native architecture of a thylakoid membrane, *Nature 430*, 1058−1062.
24. Scheuring, S., Rigaud, J. L., and Sturgis, J. N. (2004) Variable LH2 stoichiometry and core clustering in native membranes of Rhodospirillum photometricum, *EMBO J. 23*, 4127−4133.
25. Vacha, F., Bumba, L., Kaftan, D., and Vacha, M. (2005) Microscopy and single molecule detection in photosynthesis, *Micron 36*, 483−502.
26. Kirchhoff, H., Borinski, M., Lenhert, S., Chi, L., and Büchel, C. (2004) Transversal and lateral exciton energy transfer in grana thylakoids of spinach, *Biochemistry 43*, 14508−14616.
27. Gardinaru, C. C., Martinsson, P., Aartsma, T. J., and Schmidt, T (2004) Simultaneous atomic-force and two-photon fluorescence imaging of biological specimens in vivo, *Ultramicroscopy 99*, 235−245.
28. Berthold, D. A., Babcock, G. T., and Yocum, C. F. (1981) A highly resolved, oxygen-evolving photosystem II preparation from spinach thylakoid membranes, *Fed. Eur. Biochem. Soc. 134*, 231−234.
29. Porra, R. J., Thompson, W. A., and Kriedermann, P. E. (1989) Determination of accurate extinction coefficient and simultaneous equations for essaying chlorophylls a and b extracted with four different solvents: verification of the concentration of chlorophyll standards by atomic absorption spectroscopy, *Biochim. Biophys. Acta 975*, 384−394.
30. Albertsson, P. A., and Andreasson, E. (2004) The constant proportion of grana and stroma lamellae in plant chloroplasts, *Physiol. Plant 121*, 334−342.
31. Hankamer, B., Nield, J., Zheleva, D., Boekema, E., Jansson, S., and Barber, J. (1997) Isolation and biochemical characterisation of monomeric and dimeric photosystem II complexes from spinach and their relevance to the organisation of photosystem II in vivo, *Eur. J. Biochem. 243*, 422−429.
32. Kirchhoff, H., Hinz, H.-J., and Rösgen, J. (2003) Aggregation and fluorescence quenching of chlorophyll a of the light-harvesting complex II from spinach in vitro, *Biochim. Biophys. Acta 1606*, 105−116.
33. Kirchhoff, H., Mukherjee, U., and Galla, H.-J. (2002) Molecular architecture of the thylakoid membrane: Lipid diffusion space for plastoquinone, *Biochemistry 41*, 4872−4882.
34. Kaminskaya, O., Kern, J., Shuvalov, V. A., and Renger, G. (2005) Extinction coefficients of cytochromes b559 and c560 of Thermosynechococcus elongates and Cyt b559/PSII stoichiometry of higher plants, *Biochim. Biophys. Acta 1708*, 333−341.
35. Schöttler, M. A., Kirchhoff, H., and Weis, E. (2004) Photosynthetic electron transport to the carbon metabolism in tobacco, *Plant Physiol. 136*, 4265−4274.
36. Ludtke, S. J., Chen, D. H., Song, J. L., Chuang, D. T., and Chiu, W. (2004) Seeing GroEL at 6 Å resolution by single particle electron cryomicroscopy, *Structure (London) 12*, 1129−1136.
37. van Heel, M., Harauz, G., and Orlova, E. V. (1996) Single-particle electron cryo-microscopy: towards atomic resolution, *J. Struct. Biol. 116*, 17−24.
38. Dunahay, T. G., Staehelin, L. A., Seibert, M., Ogilvie, P. D., and Berg, S. P. (1984) Structural, biochemical and biophysical characterization of four oxygen-evolving photosystem II preparations from spinach, *Biochim. Biophys. Acta 764*, 179−193.
39. Nield, J., Orlova, E. V., Morris, E. P., Gowen, B., van Heel, M., and Barber, J. (2000) 3D map of the plant photosystem II supercomplex obtained by cryoelectron microscopy and single particle analysis, *Nat. Struct. Biol. 7*, 44−47.
40. Kookaburra, T., and Murata, N. (1983) Quantitative analysis of the inactivation of the photosynthetic oxygen evolution and the release of polypeptides and manganese in the photosystem III particles of spinach chloroplasts, *Plant Cell Physiol. 24*, 741−747.
41. Ghanotakis, D. F., Babcock, G. T., and Yocum, C. F. (1984) Structural and catalytic properties of the oxygen-evolving complex, *Biochim. Biophys. Acta 765*, 388−398.
42. Boekema, E. J., van Breemen, J. F.L., van Roon, H., and Dekker, J. P. (2000) Conformational Changes in photosystem II supercomplexes upon removal of extrinsic subunits, *Biochemistry 39*, 12907−12915.
43. Santos, N. C., Ter-Ovanesyan, E., Zasadzinski, J. A., Prieto, M., and Castanho, M. A. R. B. (1998) Filipin-induced lesions in planar phospholipids bilayers imaged by atomic force micsroscopy, *Biophys. J. 75*, 1869−1873.
44. Ferreira, K. N., Iverson, T. M., Maghlaoui, K., Barber, J., and Iwata, S. (2004) Architecture of the photosynthetic oxygen-evolving center, *Science 303*, 1831−1838.
45. Nield, J., Balsera, M., De Las Rivas, J., and Barber, J. (2002) Three-dimensional electron cryo-microscopy study of the extrinsic domains of the oxygen-evolving complex of spinach: assignment of the PsbO protein, *J. Biol. Chem. 277*, 15006−15012.

46. Kubitscheck, U., and Peters, R. (1998) Localization of single nuclear pore complexes by confocal scanning microscopy and analysis of their distribution, *Methods Cell Biol. 53*, 79−98.
47. Andersson, B., and Aro, E.-M. (2001) Photodamage and D1 protein turnover in photosystem II, in *Regulation in photosynthesis* (Aro, E.-M., and Andersson, B., Eds.) pp 377−393, Kluwer Academic Publishers, Dordrecht, The Netherlands.
48. Kirchhoff, H., Schöttler, M. A., and Weis, E. (2004) Plastocyanin redox kinetics in chloroplasts: Evidence for a dis-equilibirium in the high potential chain, *Biochim. Biophys. Acta 1659*, 63−72.
49. Joliot, P., and Joliot, A. (2006) Qunatification of cyclic and linear flows in plants, *Proc. Natl. Acad. Sci. U.S.A. 29*, 4913−4918.
50. Baena-Gonzalez, E., and Aro, E.-M. (2002) Biogenesis, assembly and turnover of photosystem II units, *Philos. Trans. R. Soc. London, B 357*, 1451−1460.
51. Boekema, E. J., Roon, H. van Calkoen, F., Bassi, R., and Dekker, J. P. (1999) Multiple types of association of photosystem II and its light-harvesting antenna in partially solubilized photosystem II membranes, *Biochemistry 38*, 2233−2239.
52. Kirchhoff, H., Haase, W., Wegner, S., Daniellsson, R., Ackermann, R., and Albertsson, P.-A. (2007) Low-light induced array formation of photosystem II in higher plant chloroplasts, *Biochemistry* (in press).
53. Allen, J. F. (2003) State transitions—a question of balance, *Science 299*, 1530−1532.
54. Barber, J., and Andersson, B. (1992) Too much of a good thing: light can be bad for photosynthesis, *Trends Biochem. Sci. 17*, 61−66.
55. Kühlbrandt, W., Wang, D. N., and Fujiyoshi, Y. (1994) Atomic model of plant light harvesting complex by electron crystallography, *Nature 367*, 614−621.

BI7017877